Stable Mesostructured Silicate Films Containing Nanosized Zeolite

N. Petkov,[†] S. Mintova,*[,†] B. Jean,[‡] T. H. Metzger,[‡] and T. Bein*[,†]

Department of Chemistry, University of Munich, Butenandtstrasse 5-13 (E), 81377 Munich, Germany, and European Synchrotron Radiation Facility, ESRF, BP 220, Grenoble, France

Received December 6, 2002. Revised Manuscript Received March 25, 2003

Evaporation-induced self-assembly via spin coating was employed for the formation of microporous/mesoporous composite films from preformed pure-silica MFI/ethanol and silica/CTABr/ethanol solutions. The thickness of MFI/mesoporous films is in the range of 100−400 nm depending on the different ratios between solutions containing microstructured nanoparticles and the preformed silica/surfactant assemblies forming the final coating suspensions. The structural evolution and crystal orientation of the polycrystalline films were investigated with grazing incidence diffraction (GID) at different penetration depths using synchrotron radiation. Highly ordered mesoporous films showing hexagonal arrangement of the pores and containing MFI nanocrystallites were obtained. Most of the MFI crystals are oriented with their *a*-axes (sinusoidal channels) perpendicular to the substrates and this orientation is preserved along the film thickness. The porous MFI/mesostructured film, as a function of the penetration depth (ranging from about 7.2 to 250 nm) shows less orientation of the mesostructure in the surface layer.

Introduction

Microporous and mesoporous silica films have attracted considerable attention during the past few years as promising structures for a variety of desirable applications such as catalysis supports, separation membranes, functionalized optical coatings, miniaturization of electronic devices, selective chemical sensors, dialectical coatings, and templates for growing conductive materials.[1−5] The manufacture of composite materials showing ordered micro- and mesoporosity in thin film structures can expand the technological potential in these areas. A variety of deposition strategies has been explored for the preparation of thin microporous films on different substrates, including direct crystal growth in zeolite precursor mixtures, chemical modification of the substrates, and seeding with colloidal crystals prior to further hydrothermal treatment.[6−9] Nanoscale crystals with different framework structures were assembled on the pre-modified surface of a quartz crystal microbalance and used as effective chemical sensors.[10,11] Recently, a spin-coating process has been used for the deposition of homogeneous MFI-type films by employing stable colloidal coating solutions.[12,13]

On the other hand, a rapid solvent evaporation method of preformed silica/surfactant assemblies has been introduced as a suitable technique for the preparation of continuous thin mesoporous films.[14−21] The structural evolution and the formation mechanism of these structures was thoroughly examined by time-resolved SAXS and interferometric measurements. It was shown that a variety of complex and competing process such as organization of the micellar entities, self-assembly of the organic and inorganic species, and polycondensation of the silica network, take place during the deposition of the film by dip- or spin-coating. Unfortunately, the wall structure of these materials is essentially amorphous, resulting in lower hydrothermal

* Corresponding authors. Fax: +4989 2180 77622. E-mail: svetlana.mintova@cup.uni-muenchen.de; tbein@cup.uni-muenchen.de.
[†] University of Munich.
[‡] European Synchrotron Radiation Facility.

(1) Bein, T. *Chem. Mater.* **1996**, *8*, 1636.
(2) Fan, H.; Lu, Y.; Scott, S. T.; Baer, T.; Schunk, R.; Lopez, G. P.; Brinker, C. J. *Microporous Mesoporous Mater.* **2001**, *44*−*45*, 625.
(3) Fan, H.; Lu, Y.; Stump, A.; Scott, S. T.; Baer, T.; Schunk, R.; Perez-Luna, V.; Lopez G. P.; Brinker, C. J. *Nature* **2000**, *405*, 56.
(4) Hayward, R. C.; Alberius-Henning, P.; Chmelka, B. F.; Stucky, G. D. *Microporous Mesoporous Mater.* **2001**, *44*−*45*, 619.
(5) Tavolaro, A.; Drioli, E. *Adv. Mater.* **1999**, *11*, 975.
(6) Hedlund J.; Mintova, S.; Sterte, J. *Microporous Mesoporous Mater.* **1999**, *28*, 185.
(7) Li, Q.; Hedlund, J.; Creaser D.; Sterte J. *Chem. Commun.* **2001**, 527.
(8) Erdem-Senatalar, A.; Tather, M.; Ürgen, M. *Microporous Mesoporous Mater.* **1999**, *32*, 331.
(9) Lovallo, M.; Tsapatsis, M. *AIChE J.* **1996**, *42*, 3020.
(10) Mintova, S.; Schoeman, B. J.; Valtchev, V.; Sterte, J.; Mo, S.; Bein, T. *Adv. Mater.* **1997**, *9*, 585.
(11) Mintova, S.; Mo, S.; Bein, T. *Chem. Mater.* **2001**, *13*, 901.
(12) Mintova, S.; Bein, T. *Adv. Mater.* **2001**, *13*, 1880.
(13) Wang, Z.; Mitra, A.; Wang, H.; Yan, Y. *Adv. Mater.* **2001**, *13*, 1463−1466.
(14) Lu, Y.; Ganguli, R.; Drewien, C. A.; Anderson, M. T.; Brinker, C. J.; Gong, W.; Guo, Y.; Zink, J. I. *Nature* **1997**, *389*, 364.
(15) Brinker, C. J.; Lu, Y.; Sellinger, A.; Fan, H. *Adv. Mater.* **1999**, *11*, 579.
(16) Besson, S.; Gacoin, T.; Jacquiod, C.; Ricolleau, C.; Babonneau D.; Boilot, J.-P. *J. Mater. Chem.* **2000**, *10*, 1331.
(17) Klotz, M.; Albouy, P.-A.; Ayral, A.; Menager, C.; Grosso, D.; Van der Lee, A.; Cabull, V.; Babonneau, F.; Guizard, C. *Chem. Mater.* **2000**, *12*, 1721.
(18) Besson, S.; Ricolleau, C:, Gacoin, T.; Jacquiod, C.; Boilot, J.-P *J. Phys. Chem. B* **2000**, *104*, 12095.
(19) Ogawa, M.; Masukawa, N. *Microporous Mesoporous Mater.* **2000**, *38*, 35.
(20) Ogawa, M. *J. Am. Chem. Soc.* **1994**, *116*, 7941.
(21) Ogawa, M. *Chem. Commun.* **1996**, 1149.

10.1021/cm021748e CCC: $25.00 © 2003 American Chemical Society
Published on Web 04/29/2003

stability compared to that of microporous materials, particularly zeolites, and limiting the scope of industrial applications. Obviously, a significant improvement of the physicochemical properties of the mesoporous films might be expected if the thermal stability could be improved by introduction of crystallinity into the pore walls.[22−29] One approach proposed by Kloetstra[23] is to transform pre-assembled walls of MCM-41 material into zeolitic structures by post-assembly treatment with a structure-directing template for zeolites. More recent papers have reported that the mesostructure walls can be partially converted into zeolitic product resulting in ZSM-5/MCM-41 composites.[24] The use of zeolite seeds as precursors for the assembly of steam-stable aluminosilicate mesostructures was reported by the group of Pinnavaia.[25,26] Micro- and mesoporous composite bulk materials have been synthesized in situ by using mixtures of different alkylammonium templates upon conventional or microwave hydrothermal treatment.[27−29] It has been suggested that such composite materials are potentially interesting catalysts with improved mass transport or that they serve as hosts for different sensing applications. However, to our knowledge a method for the preparation of thin films containing both ordered micro- and mesoporosity has not yet been reported.

In this study we report on the preparation of a composite MFI/MCM film on silicon wafers by employing a spin-coating process. The method relies on the evaporation-induced self-assembly of precursor acidic silica/CTABr/ethanol solutions mixed with stable MFI/ethanol colloidal suspensions. Once the coating mixture is deposited on the silicon surface, a composite film can be formed under suitable conditions with densely packed zeolite crystals.

Experimental Section

Preparation of Coating Solutions. Clear solutions containing precursor silica/surfactant assemblies were prepared by a two-step process.[14] First, acid-catalyzed hydrolysis−condensation of tetraethoxysilane (TEOS 98%, Aldrich) under reflux conditions at 60 °C for 1 h was performed followed by addition of an ethanolic solution of cetyltrimethylammonium bromide (CTAB, Aldrich) at room temperature. The final molar ratio of the precursor solution for the mesostructured phase was TEOS/CTAB/HCl/H_2O/EtOH 1:0.35:0.06:27:60 (solution M1).

Nanosized MFI crystals were synthesized from a clear precursor solution with the molar composition TPAOH/SiO_2/H_2O/EtOH 9:25:408:11 at 90 °C for 12 h (solution M2) (for details see ref 12). After the synthesis, the resulting nanosized crystals were purified twice by centrifugation (20 000 rpm, 1 h) and subsequently redispersed in double-distilled water under ultrasonication. After the second centrifugation step, the redispersion of the zeolite particles was performed in ethanol (98%, Aldrich). The concentration of the solid nanocrystals in the MFI/ethanol suspension (M2) was 3 wt %. The final coating mixtures for deposition of the MFI/mesoporous composite films were prepared from the M1 and M2 solutions with different weight ratios (Table 1).

Table 1. Coating Mixtures and Films Prepared Thereafter

sample	coating mixture MFI/mesoporous (weight ratio)	deposition steps	films
M1	0-1	1	continuous, smooth
M2	1-0	1	continuous
M1-1	1:1	1	continuous, smooth
M1-3	1:1	3	continuous, increased roughness
M2-1	2:1	1	continuous, smooth
M2-3	2:1	3	continuous, increased roughness
M3-1	3:1	1	continuous, homogeneous, smooth
M3-3	3:1	3	continuous, homogeneous
M4-1	4:1	1	no film, randomly distributed nanocrystals

Preparation of Films via Spin Coating. Composite MFI/mesoporous films, as well as pure mesoporous and pure MFI films, were deposited on silicon (Si) wafers {001}(25 × 25 mm) by spin-coating (SCS P6700 Spin coater) with a spinning rate of 2000 rpm for 35 s. All substrates were cleaned with two different solutions (ethanol and acetone) for 10 s prior to the film deposition. The substrates were vacuum-locked during the spin-coating process.

The spin-coating deposition was performed with different coating mixtures as described in Table 1. For multiple depositions of the porous layers, alternating coating and drying steps at room temperature were performed resulting in multilayer structures. Finally, the composite films were thermally stabilized at 120 °C for 6 h and calcined at 500 °C for 1 h (0.5 °C/min ramping). The pure mesoporous and the pure MFI films were calcined at 500 and 450 °C for 3 h, respectively, to remove the organic template prior to other measurements.

Characterization. The radius of the solid particles and the particle-size distribution in the coating mixtures prior to the film deposition were determined with dynamic light scattering (ALV-NBS/HPPS) and high-resolution transmission electron microscopy (HRTEM, Philips 200 FEG) operated at 200 kV. The backscattering geometry (scattering angle 173°, HeNe laser with 3 mW output power at a wavelength of 632.8 nm) permits measurements of the coating mixtures at high sample concentrations. The analyses were performed on original coating mixtures without any further pretreatment.[30] Two standard methods were applied for the characterization of all samples: (a) cumulant analysis and (b) distribution function analyses (DFA). The typical measurement settings included 30 scans, and the calculated polydispersity index (i_p) was used to indicate a multimodal particle size distribution.

The surface features of the MFI/mesoporous composites and of pure mesoporous films were investigated with atomic force microscopy (Nanoscope NSE-Digital Instruments) and scanning electron microscopy (Philips 40 XL).

Grazing incidence X-ray diffraction was used to investigate the mesophase structure and the orientation of MFI crystallites in the composite films along their thickness, and compared with those of the pure mesoporous and MFI films. The 6-circle diffractometer at beam-line ID01 at the ESRF

(22) Karlson, A.; Stocker M.; Schmidt, R. *Proc. 12th Int. Zeolite Conf.* Treacy, M. M. J., Marcus, B. K., Bisher, M. E., Higgins, J. B., Eds.; MRS: Warrendale, PA, **1998**, *1*, 713.
(23) Kloetstra, K. R.; van Bekkum, H.; Jansen, J. C. *Chem. Commun*. **1997**, 2281.
(24) Huang, L.; Guo, W.; Deng, P.; Xue Z.; Li, Q. *J. Phys. Chem. B* **2000**, *104*, 2817.
(25) Liu, Y.; Zhang W.; Pinnavaia, T. J. *Angew. Chem*. **2001**, *113*, 1295.
(26) Liu, Y.; Zhang W.; Pinnavaia, T. J. *J. Am. Chem. Soc.* **2000**, *122*, 8791.
(27) Karlson, A.; Stocker, M.; Schmidt, R. *Microporous Mesoporous Mater*. **2000**, *104*, 2817.
(28) Kim, D. S.; Park, S.-E.; Kang, S. O. *Stud. Surf. Sci. Catal. (Nanoporous Materials II, Proceedings of the Conference on Access in Nanoporous Materials)* **2000**, *129*, 107.
(29) Karlson, A.; Stocker, M.; Schafer, K. *Stud. Surf. Sci. Catal. (Nanoporous Materials II, Proceedings of the Conference on Access in Nanoporous Materials)* **2000**, *129*, 99.
(30) Mintova, S.; Petkov, N.; Karaghiosoff, K.; Bein, T. *Microporous Mesoporous Mater*. **2001**, *50*, 121.

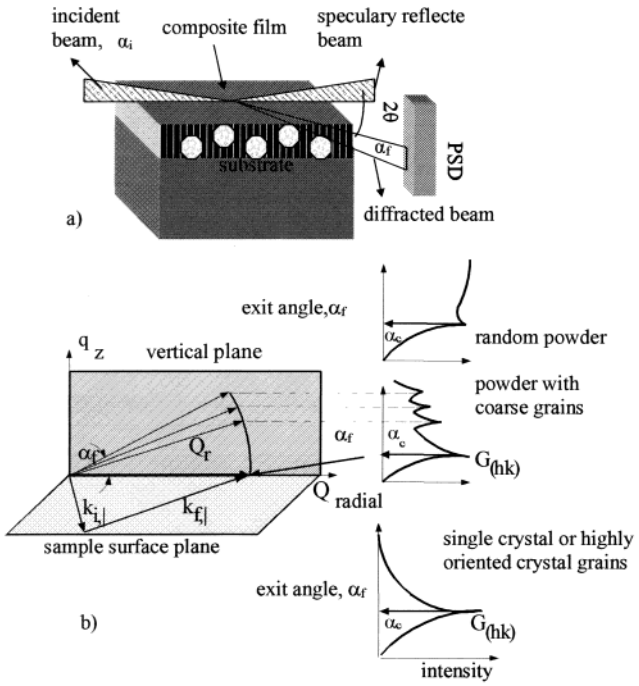

Figure 1. (a) Scattering geometry of grazing incidence diffraction (GID) where the diffraction intensity as a function of the scattering angle 2θ is recorded by a position-sensitive detector (PSD) at small angles of incidence (α_i) and exit (α_f); and (b) sketch of the scattering geometry in the reciprocal space (for details see ref 32).

(www.esrf.fr) in Grenoble, France was used for all X-ray experiments.[32] The wavelength was selected by a double crystal monochromator to $\lambda = 0.156$ nm. The accuracy in setting the incident angle was $\Delta\alpha_i = 0.005°$. The scattered signal was collected by a position-sensitive linear detector (PSD) placed 80 cm behind the sample. The footprint on the sample surface is about 0.5 × 0.5 mm given by the crossing of the parallel incident beam and the collimation of the beam behind the sample. The scattering geometry for grazing incidence diffraction (GID) is shown in Figure 1a. The incident (α_i) and exit (α_f) angles are at the order of the critical angle (α_c) for total external reflection, typically some tenths of a degree. The scattered intensity was collected at small exit angles (α_f) by PSD as a function of the scattering angle 2θ (see Figure 1a). In GID geometry only the lattice parameter of planes perpendicular to the surface can be recorded, so the α_f range of the PSD yields information on the distribution of G_{hkl} in the interval $\Delta\tau$. In our experiments, the key features of the structure of the MFI and mesoporous channel system on the silicon substrate are obtained from the specific direction measured in reciprocal space. The evaluation of the mesophase structure and texture is possible by applying small-angle GID. Most important for the texture determination of the MFI crystallinity are the Bragg reflections in the region of 7−9° and 21−23° 2θ. The orientation distribution of the corresponding channels is most directly reflected in the α_f-spectra at these specific Bragg reflections as explained above. In all composite films, the structural properties were investigated with respect to the direction normal to the substrate by changing α_i and/or α_f, thus tuning the information a depth throughout the film structure.

Results and Discussion

Coating Mixtures. The dynamic light-scattering results of the pure silica/surfactant solution (M1), the MFI/ethanol suspension (M2), and all the coating mixtures were obtained in a backscattering mode at the original concentration without dilution of the samples. DLS studies reveal that the two initial solutions M1 and M2 have particles with monomodal particle size distribution (Figure 2). The M1 solution contains particles with a hydrodynamic radius in the range of 1−10 nm (Figure 2a), which are attributed to silica oligomers and larger entities obtained after hydrolysis of TEOS in acidic media. The radius of the zeolite crystals in solution M2 is estimated to be around 40 nm (Figure 2b). In addition, the small polydispersity indexes calculated from the cumulant analysis, $i_p = 0.08$ and 0.02, are consistent with the monomodal particle size distribution of samples M1 and M2, respectively. A TEM micrograph of the pure MFI particles reveals their small size and platelike shape with visible crystalline faces (inset in Figure 2). The size of the nanocrystals determined from the TEM image is consistent with the particle radii measured with the DLS technique. After mixing of the solution M1 and suspension M2 to obtain the coating mixture M3-1 (see Table 1), new particles are formed with a mean hydrodynamic radius of around 60 nm (Figure 2c). The particle size distribution of this coating mixture does not change with time (at least one week); this confirms its colloidal stability at ambient temperature. The difference between the mean particle radius in the M2 suspension (∼40 nm) and in the coating mixture (∼60 nm) is probably due to the formation of a mesoporous silica shell around the MFI zeolite crystals, formed from the silicate oligomers existing in the solution M1 (1−10 nm). All as-prepared coating mixtures (Table 1) consisting of the M1 and M2 samples were stable with time; no sedimentation was observed during one week at ambient temperature. However, fresh coating mixtures were prepared prior to the film-deposition experiments. When the weight ratio of the MFI suspension in the final coating mixtures is increased to 4:1 or greater, the coating solutions are no longer stable and precipitate after several minutes.

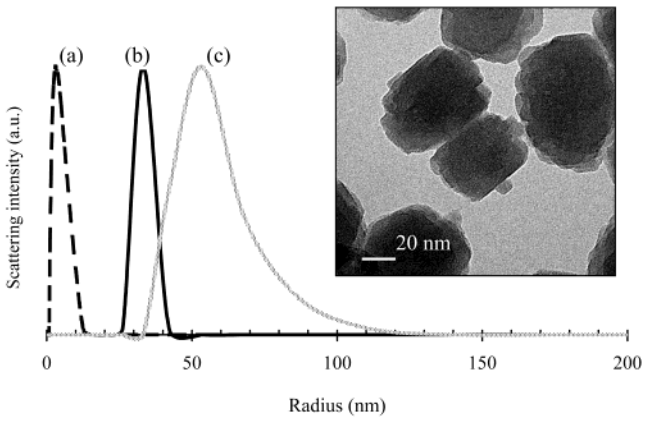

Figure 2. DLS data of (a) silica/surfactant solution (M1), (b) MFI/ethanol suspension (M2), and (c) coating mixture consisting of M1 and M2 (M3-1). The distribution function analysis data are displayed as scattering intensity per relative mass content.

MFI/Mesoporous Films Prepared via Spin Coating. To confirm the mesophase structure together with the orientation of the MFI crystallites in the composite film, grazing angle X-ray diffraction measurements were undertaken. A structural comparison was made with the

(31) Hillhouse, H.; van Egmond, J. W.; Tsapatsis, M.; Hanson, J.C; Lareze, J. Z. *Microporous Mesoporous Mater.* **2001**, *44*−*45*, 639.
(32) Metzger, T. H.; Mintova, S.; Bein, T. *Microporous Mesoporous Mater.* **2001**, *43*, 191.

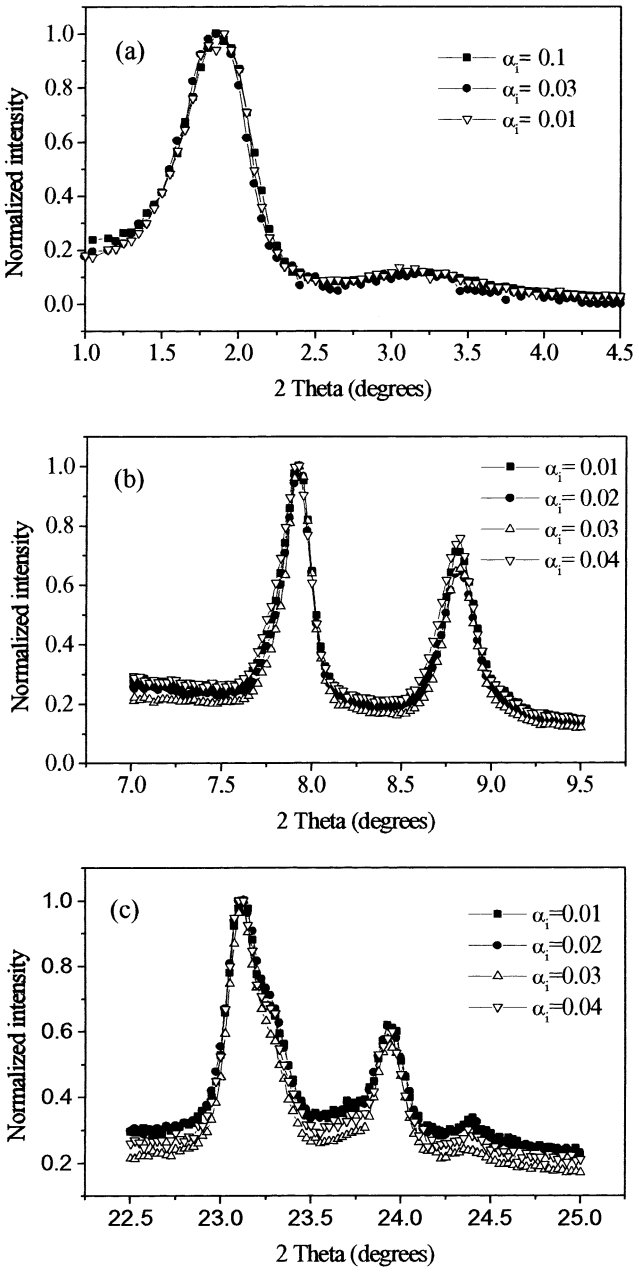

Figure 3. Radial 2θ scans of calcined (a) mesoporous film prepared from solution M1 in the 2θ range of 1.0−4.5°; and MFI film prepared from solution M2 in the 2θ ranges of (b) 7.0−10.0° and (c) 22.0−25.0°. The angle of incidence is in the range of $\alpha_i = 0.01-0.1°$ and $\alpha_i = 0.01-0.04°$ for the mesoporous and MFI films, respectively.

films prepared from coating solutions that led to pure mesostructured and pure MFI films. The films were investigated as a function of depth in the growth direction by changing α_i and/or α_f, thus tuning the information depth through the layer structure.

The mesophase structure of the film prepared from the M1 coating solution (without MFI nanoparticles) is deduced from the scans over all exit angles seen by the PSD. The region of interest is set from 1° to 4.5° 2θ where the expected Bragg diffractions appear for the mesoporous materials. The incident angle (α_i) was varied from 0.01° to 0.1° and the scattered intensities of the Bragg reflections are given in Figure 3a. For the film M1, two diffraction peaks were recorded at 1.86° and 3.14° 2θ that were assigned to the (100) and (110) planes of the *p*6*m* hexagonal mesophase structure. Because in the GID geometry only the lattice parameter of planes parallel to the surface can be recorded, we assume that the hexagonal organization of the mesophase structure shows at least some channels oriented perpendicular to the substrate surface. The unit cell parameter of the hexagonal mesostructure [$a = 2/3^{1/2}\, d_{(100)}$] is determined to be $a = 55.1$ Å. The half-width of the Bragg peak calculated from a Lorentzian fit is 0.51° 2θ. This value and the peak position do not change with the variation of the incident angle, showing one and the same mesophase structure along the film thickness.

The measurement of the pure MFI microporous film (M2) shows that (−101/011), (020), (051), and (−303/033) Bragg peaks appear (Figure 3b and c); this finding, combined with additional intensity differences compared to those of powder samples, reveals that the crystals are preferentially oriented with the *a*-axes perpendicular to the substrate surface. The measurements at different α_i from 0.05° to 0.3° show that the intensity of the Bragg reflections does not change, indicating that the crystals have the same orientation along the film thickness.

Experimental results for MFI/mesoporous composite film prepared from the M3-1 coating mixture are shown in Figure 4. Two-theta scans were collected at incident angles varied from 0.15° to 0.4° (i.e., around the α_c) and the Bragg peaks are given in Figure 4a. In the mesopore region, two reflections were detected: the first one at 1.87° 2θ and its first harmonic at 3.7° 2θ. These two Bragg peaks are indexed as first- and second-order reflection of the lattice planes parallel to the substrate characteristic of the *p*6*m* hexagonal mesophase structure. In depth-sensitive measurements, the first very intensive and second less intensive reflections always appeared at the same 2θ positions, while the intensity was decreased only at the lowest incident angle α_i = 0.15°, and this result suggests lower order of crystals at the film surface. The corresponding measurements of the same sample in the angular ranges 2θ = 6.5−9.5° and 22−25° (associated with MFI) are shown in Figure 4b and c. The measurements at different α_i show that only the Bragg reflections at 7.94°, 8.90°, 23.1°, and 23.98° 2θ with *hkl* of (011), (020), (051), and (033), respectively, are observed. In this case only reflections with *hkl* values having $h = 0$ are recorded, which reveals that the crystals are oriented with the *a*-axes perpendicular to the substrate surface. These measurements permit an investigation of the porous structure as a function of the penetration depth, ranging from about 7.2 nm at α_i = 0.05° to 250 nm at α_i = 0.3°.[34] A large fraction of the crystals in the top layer at α_i = 0.05° are oriented with their *a*-axes perpendicular to the substrate surface ($h = 0$), and at α_i = 0.3° all these reflections become even sharper and better defined. The Bragg peaks found in both angular ranges characteristic for MFI-type zeolite show the same orientation behavior.

Depth-dependent structural information on a certain lattice plane is obtained by keeping the corresponding

(33) Treasy, M. M. J.; Higgins, J. B. *Collection of Simulated XRD Powder Patterns of Zeolites, 4th revised edition*; Elsevier: New York, 2001, pp 236−237.

(34) Mintova, M., Metzger, T. H., Bein, T., *Stud. Surf. Sci. Catal. "Zeolites and Mesoporous Materials at the Dawn of the 21st Century"* **2001**, *135*, 3160.

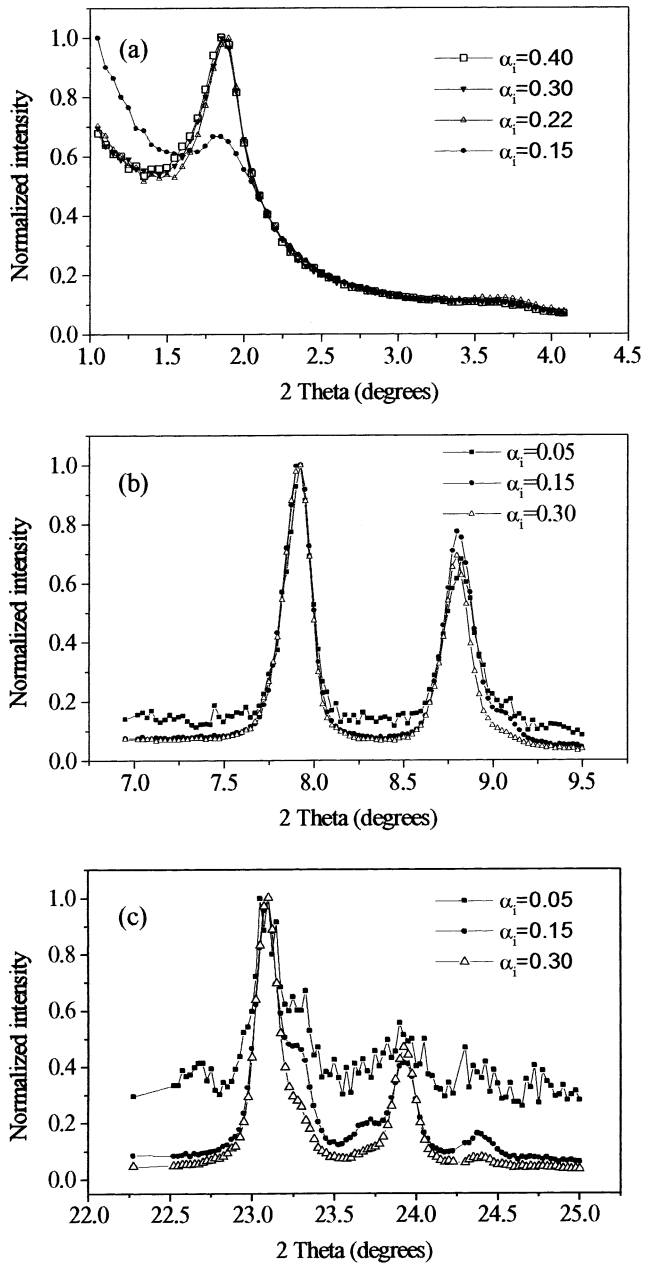

Figure 4. Radial 2θ scans of calcined composite MFI/mesoporous film prepared from solution M3-1 in the 2θ ranges (a) 1.0−4.0°; (b) 7.0−10.0°; and (c) 22.0−25.0°.

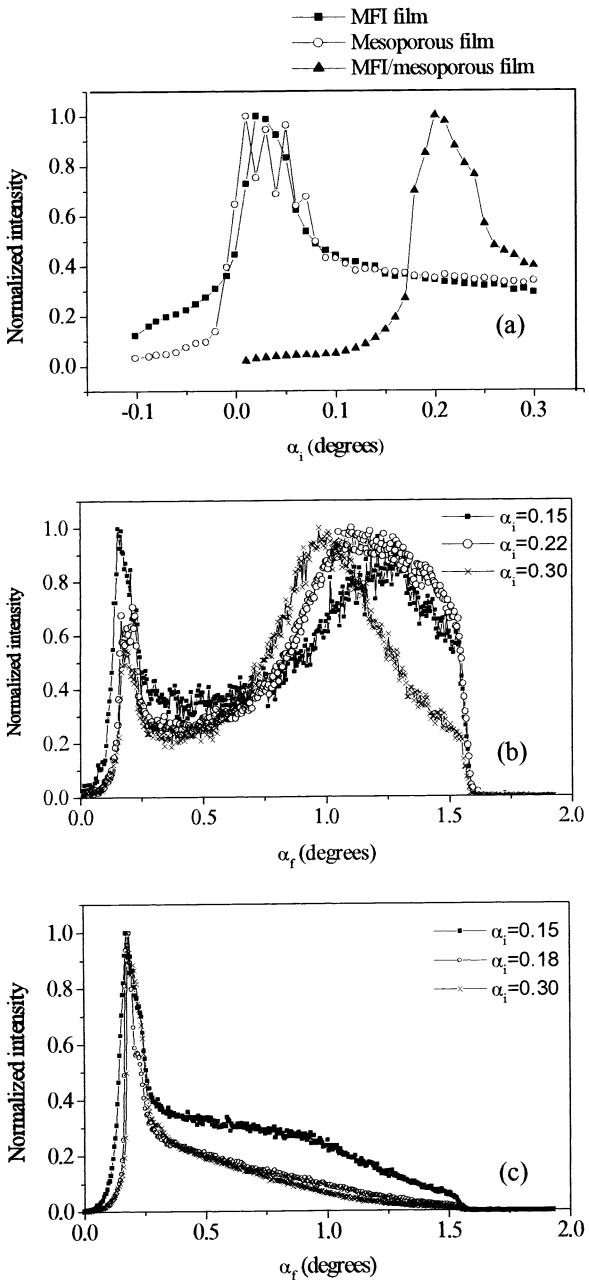

Figure 5. The α_i-dependent intensity distribution for (a) MFI (7.94° 2θ), mesoporous (1.87° 2θ), and MFI/mesoporous composite (7.94° 2θ) films prepared from solutions M2, M1, and M3-1, respectively; (b) α_f-dependent intensity distribution of the MFI/mesoporous composite film at 1.87° 2θ measured at different incident angles; and (c) α_f-dependent intensity distribution of the MFI/mesoporous composite film at 7.94° 2θ (hkl = 011) measured at different incident angles.

$2\theta_{(hkl)}$ constant and varying α_i. The intensity of Bragg peaks at 1.87° (mesoporous peak) and 7.94° (MFI peak) as a function of the incident angle for M1, M2, and M3-1 samples is depicted in Figure 5. Considering the density of a layer is related to the position of the critical angle, the multiple maxima found for sample M1 indicate depth fluctuation in the layer density, corresponding to angles between 0.01° and 0.1°. A similar measurement for sample M2 (filled square symbol in Figure 5) shows a smoother distribution of the intensity as a function of α_i with pronounced maxima at the critical angle (α_c = 0.05°). This curve is characteristic for single crystals, where all lattice planes of the corresponding Bragg peak are oriented perpendicular to the substrate, thus G^1_{hkl} is placed parallel to the sample surface. The width along α_i is determined by structural effects such as a finite angular distribution of the lattice planes along the direction perpendicular to the sample surface.[32] Surprisingly, the intensity distribution in the same α_i region for the MFI/mesoporous composite film shows a shift in the maximum intensity toward higher incident angles. This indicates increased density of the deposited layer in comparison to those of the pure mesoporous and pure MFI films.

The best depth sensitivity is, however, reached when the intensity distribution along the exit angles (α_f) is investigated. Here α_i and 2θ are kept constant and the α_f-intensity distribution is recorded (Figure 5b and c). For different α_i, the α_f spectra reflect the distribution of orientation of the crystallites as a function of depth. In Figure 5b and c the α_f-spectra at three α_i values are

shown for the composite film M3-1 at the 1.87° 2θ reflection characteristic for the mesophase, and at the 7.94° 2θ reflection typical for the presence of MFI type nanoparticles. The intensity is normalized to the maximum to demonstrate the functional dependence with respect to α_f. At the (100) peak of the mesoporous phase the α_f distribution of the intensity shows a pronounced peak at $\alpha_f = 0.19°$ and a broad enhancement of the intensity centered at $\alpha_f = 1.5°$. Going back to Figure 1b, one can see in the upper panel how the α_f intensity-distribution will look if the ordered domains have all possible orientations, such as a random powder. The Bragg intensity increases for $0 < \alpha_f < \alpha_c$ and the maximum is dominated by the transmission function. The further increase of the intensity corresponds to the scattering of the disordered domains forming a wormlike structure with no preferred orientation. Similar results have been reported about CTAB−silica films prepared by dip-coating and additionally visualized with the TEM images collected on film cross-sections.[35] The depth profile (α_f intensity distributions taken at different $\alpha_i = 0.15-0.3°$ shows similar behavior for all α_i, again indicating that the mesophase structure exhibits a similar orientational disorder along the thickness of the layer. Apparently, the common horizontal orientation of channels in MCM-41 films is modified by the presence of the colloidal zeolites. In the case of the (011) reflection characteristic for the MFI nanocrystals, the α_f spectra again exhibit a pronounced maximum indicating the preferred orientation of the microporous sinusoidal channels of MFI-type zeolite nanocrystals. In addition, the orientation is better in the deeper layers of the sample since the peak has a well-shaped maximum at $\alpha_i = 0.3°$. The scan at $\alpha_i = 0.15°$ gives a penetration depth of about 10.5 nm, whereas at $\alpha_i = 0.3°$ it is about 250 nm. All curves are almost identical, which shows that the straight channels are well-oriented perpendicular to the surface along the thickness of the film.

The structural difference between pure mesoporous and MFI/mesoporous composite films can be explained by the seeding effect of the colloidal MFI-type nanocrystals that change the nature of the self-assembly process of the micellar species and silica oligomers during the film deposition. In the first case the rapid solvent evaporation induces formation of a highly ordered hexagonal mesostructure with preferred orientation of the channels with *c*-axes parallel to the substrate surface. In the case of the MFI/mesoporous composite film, the existence of colloidal microporous crystals in the coating mixture distorts the self-assembly process and leads to the formation of tubular micellar species that self-assemble in a two-dimensional hexagonal pattern, showing a mosaic-type distribution of the ordered domains. In the near vicinity of the MFI nanocrystals, the distortion of the mesophase channel arrangement probably leads to the formation of a wormlike mesophase structure.

Microscopic Investigation of MFI/Mesoporous Films. SEM investigations of the pure MFI, mesoporous, and composite films were performed to investigate the thickness of the layers, and their surface morphology and homogeneity. The pure mesoporous film (Figure 6a) exhibits very homogeneous surface morphology with no special surface features on a nanometer scale. The top-view image of this mesoporous film is taken at a scratched part of the film to make focusing possible (Figure 6a). The surface features of all composite films prepared from the coating mixtures are summarized in Table 1. Figure 6b shows the SEM top-view image of the MFI/mesoporous film prepared from coating mixture M3-1. Homogeneous and continuous film at a centimeter scale is obtained by one-step spin coating. The homogeneity of the deposited layer is preserved by the close packing of the MFI-type nanocrystals surrounded by mesoporous material. No open space between individual crystallites is detected in the MFI/mesoporous composite films (Figure 6b), due to a layer of mesoporous phase between the MFI crystalline grains. The thickness of this film (side-view) is about 100 nm (Figure 6c). After two or three spin-coating deposition steps of the same mixture, a thicker film is obtained that is again continuous across the Si substrates.

The MFI/mesoporous composite films prepared from coating mixture M1-1 and M1-3 after one- and three-step depositions, respectively, are shown in Figure 6d and e. The films appear more rough with slight corrugations and uneven features on a nanometer scale; here the nanosize particles are embedded in a continuous matrix of mesoporous material. The perfect packing of the MFI nanoparticles is now lost, and the amount of the mesoporous material surrounding the zeolite nanoparticles is enlarged due to the increased mass fraction of the silica/surfactant solution in the coating mixture (see Table 1). A film prepared from coating solution M1-3 shows enhanced surface roughness, and additional micrometer-size openings are detected all over the film. The increased surface roughness of the multilayered films could be explained by the higher surface roughness of the intermediate porous layers in comparison to that of the bare Si wafer. When the weight ratio of the MFI suspension in the coating mixtures reached 4:1, no continuous composite films were obtained; only islands of porous nanocrystals with inhomogeneous appearance along the Si wafers were observed. This is consistent with the low stability of the coating solution (M4-1) upon mixing of the MFI suspension and silica/surfactant/ethanol solution. Fast agglomeration of the MFI nanoparticles resulting in sedimentation on the bottom of the container was detected while keeping the M4-1 coating solution at room temperature.

AFM measurements were carried out in a contact mode to elucidate the surface morphology of the calcined composite films prepared from M1 and M3-1 coating mixtures (Figure 7). The AFM image of the calcined pure mesoporous film shows an extremely smooth surface with film roughness less than 10 nm typical for CTABr templated mesoporous films prepared by spin coating. The film roughness of the composite MFI/mesoporous film is evaluated to be less than 50 nm and results from the introduction of the MFI nanocrystals. The MFI colloidal crystals appear to be homogeneously distributed in the composite film, and no voids between individual "packed-packaged" crystallites are formed.

(35) Grusso, D.; Babonneau, F.; Albouy, P.-A., Amenitsch, H., Balkenende, A. R.; Brunet-Bruneau, A.; Rivory, J. *Chem. Mater.* **2002**, *14*, 931.

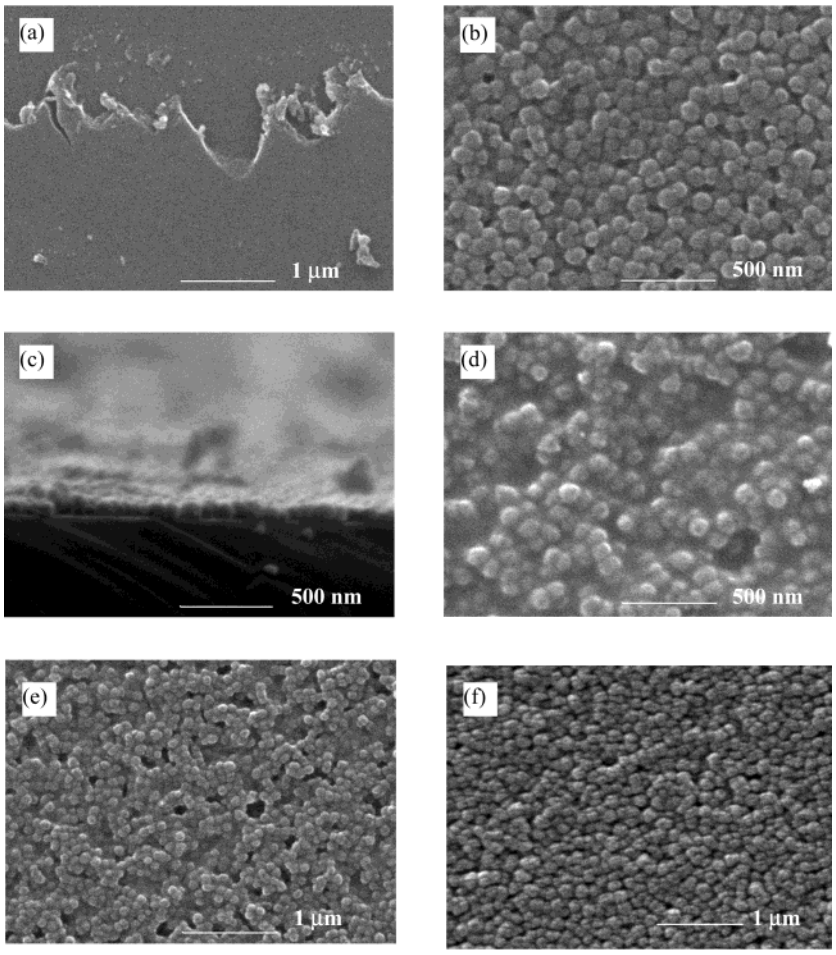

Figure 6. SEM images of the (a) pure mesoporous film (solution M1); (b) MFI/mesoporous film (solution M3-1); (c) side-view of MFI/mesoporous film (solution M3-1); (d) MFI/mesoporous film (solution M1-1); (e) MFI/mesoporous film (solution M1-3); and (f) MFI film (solution M2).

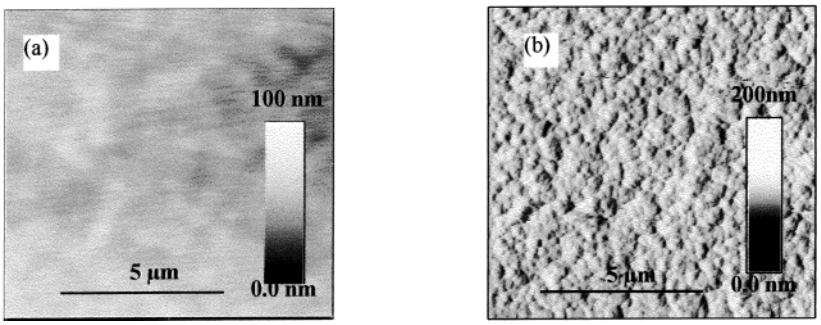

Figure 7. AFM images of (a) pure mesoporous film (solution M1) and (b) MFI/mesoporous film (solution M3-1).

Conclusion

The present paper reports on the preparation of thin films on Si wafers possessing micro- and mesoporosity. The use of stable nanosized zeolite crystals together with precursor silica/surfactant solutions is not limited to the preparation of pure silica films. The crystal orientation in the MFI/mesoporous composite films containing micro- and mesophases in comparison with the pure mesophase and pure MFI films is investigated with grazing incidence diffraction using synchrotron radiation. The loading of the mesoporous film with MFI nanoparticles provokes distortion of the ordered hexagonal structure and makes possible the existence of regions having an orientation of the mesoporous channel system different from that already observed for CTABr templated mesoporous films. The penetration-depth measurements on optimized films (M3-1) confirm that there are no changes in the orientation of the porous MFI nanocrystallites. The GID experiments show that most of the MFI zeolite crystallites are oriented with the *a*-axis perpendicular to the Si surface and the mesoporous phase does not change its average orientation along the film thickness.

The method described here is suitable for the fabrication of composite films with controlled bimodal porosity for applications requiring gentle processing conditions, and accessible pore systems for further use in host−guest chemistry or catalysis.

Acknowledgment. We thank N. Olson for the TEM photograph. Support from ESRF, Grenoble-France, DFG, (SFB486), and BFHZ is gratefully acknowledged.

CM021748E